Phase and amplitude evolution in the network of triadic interactions of the Hasegawa-Wakatani system

N.B. When citing this work, cite the original published paper.

(article starts on next page)

Phase and amplitude evolution in the network of triadic interactions of the Hasegawa–Wakatani system

Ö. D. Gürcan, J. Anderson, S. Moradi, et al.

View Online   Export Citation   CrossMark

ARTICLES YOU MAY BE INTERESTED IN

Phase and amplitude evolution in the network of triadic interactions of the Hasegawa–Wakatani system

View Online   Export Citation   CrossMark

Ö. D. Gürcan,[1,a] [ID] J. Anderson,[2,b] [ID] S. Moradi,[3,c] [ID] A. Biancalani,[4,d] [ID] and P. Morel[1,e] [ID]

AFFILIATIONS

[1]Laboratoire de Physique des Plasmas, CNRS, IP Paris, Université Paris-Saclay, 91128 Cedex, Palaiseau, France
[2]Department of Space, Earth and Environment, Chalmers University of Technology, SE-412 96 Göteborg, Sweden
[3]Laboratory for Plasma Physics, LPP-ERM/KMS, Royal Military Academy, 1000 Brussels, Belgium
[4]Léonard de Vinci, Pôle Universitaire, Research Center, 92916 Paris La Défense, France

[a]Author to whom correspondence should be addressed: ozgur.gurcan@lpp.polytechnique.fr
[b]johan.anderson@chalmers.se
[c]sara.moradi@ukaea.uk
[d]alessandro.biancalani@devinci.fr
[e]pierre.morel@lpp.polytechnique.fr

ABSTRACT

The Hasegawa–Wakatani system, commonly used as a toy model of dissipative drift waves in fusion devices, is revisited with considerations of phase and amplitude dynamics of its triadic interactions. It is observed that a single resonant triad can saturate via three way phase locking, where the phase differences between dominant modes converge to constant values as individual phases increase in time. This allows the system to have approximately constant amplitude solutions. Non-resonant triads show similar behavior only when one of its legs is a zonal wave number. However, when an additional triad, which is a reflection of the original one with respect to the y axis is included, the behavior of the resulting triad pair is shown to be more complex. In particular, it is found that triads involving small radial wave numbers (large scale zonal flows) end up transferring their energy to the subdominant mode which keeps growing exponentially, while those involving larger radial wave numbers (small scale zonal flows) tend to find steady chaotic or limit cycle states (or decay to zero). In order to study the dynamics in a connected network of triads, a network formulation is considered, including a pump mode, and a number of zonal and non-zonal subdominant modes as a dynamical system. It was observed that the zonal modes become clearly dominant only when a large number of triads are connected. When the zonal flow becomes dominant as a "collective mean field," individual interactions between modes become less important, which is consistent with the inhomogeneous wave-kinetic picture. Finally, the results of direct numerical simulation are discussed for the same parameters, and various forms of the order parameter are computed. It is observed that nonlinear phase dynamics results in a flattening of the large scale phase velocity as a function of scale in direct numerical simulations.

Published under an exclusive license by AIP Publishing. https://doi.org/10.1063/5.0089073

I. INTRODUCTION

The Hasegawa–Wakatani model[1] was initially devised as a simple, nonlinear model of dissipative drift wave turbulence in tokamak plasmas. It has the same nonlinear structure as the passive scalar turbulence[2]—with vorticity evolving according to 2D Navier–Stokes equations—or more complex problems such as rotating convection.[3,4] From a plasma physics perspective, it can be considered as the minimum non-trivial model for plasma turbulence since it has (i) linear instability (e.g., Hasegawa–Mima model does not[5]), (ii) finite frequency (so that resonant interactions are possible[6]), and (iii) a proper treatment of zonal flows.[7] The model is well known to generate high levels of large scale zonal flows, especially for $C \gtrsim 1$,[8–10] where C is the adiabaticity parameter. It has been studied in detail for many problems in fusion plasmas including dissipative drift waves in tokamak edge,[11,12] subcritical turbulence,[13] trapped ion modes,[14] intermittency,[15,16] closures,[17–19] feedback control,[20] information geometry,[21] and machine learning.[22] Variations of the Hasegawa–Wakatani model are regularly used for describing turbulence in basic plasma devices.[23–25]

Two dimensional Hasegawa–Wakatani equations[1] with proper zonal response consist of an equation of plasma vorticity,

$$\frac{\partial}{\partial t}\nabla^2\Phi + \hat{z}\times\nabla\Phi\cdot\nabla\nabla^2\Phi = C(\tilde{\Phi} - \tilde{n}) + D_\Phi(\nabla^2\Phi), \quad (1)$$

and an equation of continuity,

$$\frac{\partial}{\partial t}n + \hat{z}\times\nabla\Phi\cdot\nabla n + \kappa\partial_y\Phi = C(\tilde{\Phi} - \tilde{n}) + D_n(n), \quad (2)$$

with the $E\times B$ velocity defined as $\boldsymbol{v}_E = \hat{z}\times\nabla\Phi$ in normalized form and $\tilde{\Phi} = \Phi - \langle\Phi\rangle$, where $\langle\Phi\rangle$ denotes averaging in y (i.e., poloidal) direction. Here, n is the fluctuating particle density normalized to a background density n_0, Φ is the electrostatic potential normalized to T/e, κ is the diamagnetic velocity normalized to speed of sound, C is the so-called adiabaticity parameter, which is a measure of the electron mobility, and D_Φ and D_n are dissipation functions for vorticity and particle density, respectively. For fluctuations, we have $D_\Phi(\nabla^2\tilde{\Phi}) = \nu\nabla^4\tilde{\Phi}$ from kinematic viscosity, whereas for the zonal flows, $D_\Phi(\nabla^2\bar{\Phi}) = -\nu_{ZF}\nabla^2\bar{\Phi}$ from large scale friction. Unless the system represents a renormalized formulation, D_n should actually be zero; however, here we include it for completeness and numerical convenience and take it to have the same form as the vorticity dissipation with diffusion $D_n(\tilde{n}) = D\nabla^2\tilde{n}$ and particle loss $D(\bar{n}) = -D_{ZF}\bar{n}$.

Formation of large scale structures, in particular, zonal flows in drift wave turbulence, is one of the key issues in the study of turbulence in fusion plasmas, which can be formulated in terms of modulational instability of either a gas of drift wave turbulence using the wave kinetic formulation[26] or a small number of drift modes,[27] resulting in various forms of complex amplitude equations such as the celebrated nonlinear Schrödinger equation (NLS).[28] It is also common to talk about zonal flows as resulting from a process of inverse cascade[29,30] and their back reaction on turbulence[31,32] resulting in predator-prey dynamics, possibly leading up to the low to high confinement transition in tokamaks.[33,34] While the role of the complex phases in nonlinear evolution of the amplitudes, especially in the context of structure formation, for example, as in the case of soliton formation in NLS, was always well known, its particular importance for zonal flow formation in toroidal geometry has only been underlined recently.[35]

Here, we revisit the Hasegawa–Wakatani system, with proper zonal response, as a minimum system that allows a description of zonal flow formation in drift wave turbulence, and study interactions between various number of modes from three wave interactions to the full spectrum of modes described by direct numerical simulations, focusing, in particular, on phase dynamics and the possibility of phase locking and synchronization. The detailed dynamics of three wave interactions[36] or the transition from a single interacting triad to a "network" of interacting triads[37,38] has been studied in the past in similar reduced models. It was also shown that synchronization of phase dynamics can lead to interesting phenomenon, such as formation of coherent structures in simple Vlasov–Poisson system.[39] In contrast, in the Hasegawa–Wakatani case, it turns out that while resonant three wave interactions involving unstable and damped modes favor phase locking (i.e., a state where the differences between individual phases remain roughly constant as they increase together), interactions involving zonal flows (i.e., four wave interactions including the triad reflected with respect to the y axis) seem to have a complicated set of possible outcomes depending on whether the zonal flow wave number

is larger or smaller than the pump wave-number. It therefore becomes critical to study a network of connected triads in order to see the collective effects of a number of triads on the evolution of zonal flows and of the relative phases between modes. Two different network configurations are considered: that with a single k_y and multiple q's, and that with a single q and multiple k_y's. Note that the algorithm that we use computes all possible interactions between the modes in a given collection of triads and then computes the interaction coefficients and evolves the system nonlinearly according to those.

Finally, we consider the results from direct numerical simulations (DNS) using a pseudo-spectral 2D Hasegawa–Wakatani solver. The DNS and the network models correspond exactly in the sense that if we consider an $N_x \times N_y$ grid and consider all the possible triads in such a grid and solve this problem using our network solver, we obtain exactly the same problem (including the boundary conditions that are periodic) as the DNS. The results of the DNS show qualitatively similar behavior to the two network models that we considered. However, looking at the evolution of phases, we observe a nonlinear flattening of the phase velocity for large scales computed as a function of x, suggesting nonlinear structure formation in the classical sense of nonlinearity balancing dispersion resulting in a constant velocity propagation at least for large scale structures. These vortex-like structures that move at a constant velocity are also clearly visible in the time evolution of density and vorticity fields.

Another interesting observation is that when we consider a network with a range of radial wave-numbers, such that some of the modes within that range are linearly unstable, it only saturates if the range also includes some wavenumbers for which the linear growth rate of the primary mode (i.e., not the damped mode) actually becomes negative. This suggests that drift wave turbulence (at least as described by the Hasegawa–Wakatani system) does not saturate "locally" by coupling to the damped modes, but transfers energy to scales where the damping of the primary mode is significant. However, since the linear growth of the primary mode for large k_x modes does not come directly from dissipation, but from the form of the dispersion relation, including the effects of dissipation, this is still different from the Kolmogorov picture where the injection and dissipation scales are well separated. Therefore, it is important to note that plasma turbulence as well as other similar systems generates and dissipate energy anisotropically in scales that are much closer to one another even though they may display power law scalings.[6,40]

The rest of the paper is organized as follows. In the remainder of the Introduction, the Hasegawa–Wakatani system is reformulated in terms of its linear eigenmodes and the amplitude and phase equations for these eigenmodes, writing out explicitly the nonlinear terms that appear in this formulation. In Sec. II, different types of interactions among dissipative drift waves are considered using these linear eigenmodes, starting with the basic three wave interaction. After showing that there is no qualitative difference between a near resonant and an exactly resonant (within numerical accuracy) triad, the details of the phase dynamics of such a single triad are discussed. In Sec. III, the interaction with zonal flows is considered. It is noted that when we consider a triad and its reflection with respect to its pump wavenumber together as a pair, the behavior of the system is qualitatively different from the single triad case. After a discussion of order parameters for this system, a network formulation is considered, and the results from such a network model are presented. Finally, the results

from direct numerical simulations of the Hasegawa–Wakatani system are discussed and compared with those earlier results based on reduced number of triads. Section IV details the conclusion.

A. Linear eigenmodes

We can write the Hasegawa–Wakatani system in Fourier space for non-zonal modes (i.e., $k_y \neq 0$) using the notation $\Phi_\mathbf{k} \rightarrow \Phi_k$ for the Fourier coefficients as follows:

$$\partial_t \Phi_k + (A_k - B_k)\Phi_k = \frac{C}{k^2} n_k + N_{\Phi k}, \tag{3}$$

$$\partial_t n_k + (A_k + B_k)n_k = (C - i\kappa k_y)\Phi_k + N_{nk}, \tag{4}$$

where

$$A_k = \frac{1}{2}\left[(Dk^2 + C) + \left(\frac{C}{k^2} + \nu k^2\right)\right] \tag{5}$$

and

$$B_k = \frac{1}{2}\left[(Dk^2 + C) - \left(\frac{C}{k^2} + \nu k^2\right)\right], \tag{6}$$

and defining

$$N_{nk} = \frac{1}{2}\sum_\triangle \hat{\mathbf{z}} \times \mathbf{p} \cdot \mathbf{q}\left(\Phi_p^* n_q^* - \Phi_q^* n_p^*\right) \tag{7}$$

and

$$N_{\Phi k} = \frac{1}{2}\sum_\triangle \frac{\hat{\mathbf{z}} \times \mathbf{p} \cdot \mathbf{q}(q^2 - p^2)\Phi_p^* \Phi_q^*}{k^2}, \tag{8}$$

where superscript $*$ denotes complex conjugation and $k^2 = k_x^2 + k_y^2$ as usual and the sum over triangle notation indicates a sum over the wave-vectors p and q satisfying the triad interaction condition $\mathbf{k} + \mathbf{p} + \mathbf{q} = 0$. Note that since the initial fields in x, y space are real, we have $\Phi_\mathbf{k}^* = \Phi_{-\mathbf{k}}$.

Diagonalizing the linear terms, we can write

$$\partial_t \xi_k^\pm + i\omega_k^\pm \xi_k^\pm = N_{\xi k}^\pm \tag{9}$$

for the two eigenmodes $\xi_k^\pm$ with the corresponding complex eigenfrequencies $\omega_k^\pm = \omega_{rk}^\pm + i\gamma_k^\pm$ that can be written as

$$\omega_k^\pm = \Omega_k^\pm - iA_k, $$

with

$$\Omega_k^\pm = \pm\left(\sigma_k\sqrt{\frac{H_k - G_k}{2}} + i\sqrt{\frac{H_k + G_k}{2}}\right), \tag{10}$$

where $\sigma_k = \text{sign}(\kappa k_y)$,

$$H_k = \sqrt{G_k^2 + C^2\kappa^2 k_y^2/k^4}, \tag{11}$$

and

$$G_k \equiv \left(B_k^2 + \frac{C^2}{k^2}\right). \tag{12}$$

This allows us to write the two linear eigenmodes as

$$\xi_k^{s_k} = n_k + \frac{k^2}{C}\left[B_k - i\Omega_k^{s_k}\right]\Phi_k, \tag{13}$$

where $s_k = \pm$. The nonlinear terms on the right hand side of Eq. (9) are thus

$$N_{\xi k}^{s_k} = N_{nk} + \frac{k^2}{C}\left(B_k - i\Omega_k^{s_k}\right)N_{\Phi k}, \tag{14}$$

and the inverse transforms can be written as

$$\Phi_k = \frac{i}{2}\frac{C}{k^2}\sum_{s_k} \frac{\xi_k^{s_k}}{\Omega_k^{s_k}}, \tag{15}$$

$$n_k = -\frac{i}{2}\sum_{s_k} \frac{1}{\Omega_k^{s_k}}\left(B_k + i\Omega_k^{s_k}\right)\xi_k^{s_k}. \tag{16}$$

Considering the inviscid limit, $\{D, \nu\} \rightarrow 0$ and $k_y \rightarrow O(\epsilon)$, where ϵ is a smallness parameter, and keeping terms only up to $O(\epsilon)$, we obtain

$$\xi_k^+ \approx n_k + \left(k^2 - i\frac{\kappa k_y}{2A_k^2}\right)\Phi_k, \tag{17}$$

$$\xi_k^- \approx n_k - \left(1 + i\frac{\kappa k_y}{2A_k^2}\right)\Phi_k, \tag{18}$$

which means that one could loosely refer to these two eigenmodes as the potential vorticity mode (i.e., $\xi_k^+ \sim n_k + k^2\Phi_k$) and the non-adiabatic electron density mode (i.e., $\xi_k^- \sim n_k - \Phi_k$), somewhat similar to the real space decomposition used in Ref. 41. Since the equations are already diagonal for $k_y = 0$ modes, we can use $\xi_k^+ = k^2\Phi_k$ and $\xi_k^- = n_k$ for those (or $\bar{\Phi}_k$ and $\bar{n}_k$ explicitly as we will do below).

Notice that the two eigenmodes in Eq. (13) are not orthogonal. They have the same frequencies (in opposite directions) but different growth rates with $\gamma_k^+ > \gamma_k^-$ (with $\gamma_k^- < 0$, while γ_k^+ can be positive or negative depending on the wave-number). The full nonlinear initial value problem can be solved as follows: We first compute $\xi_k^{s_k}(0)$ (i.e., $\xi_k^{s_k}(t)$ at $t = 0$) from Eq. (13) using the initial fields $n_k(0)$ and $\Phi_k(0)$. Then we advance those to $\xi_k^{s_k}(t)$ using Eq. (9), where the linear matrix is now diagonal (but the nonlinear coupling terms are rather complicated). Finally, we go back to compute $\Phi_k(t)$ and $n_k(t)$ using Eqs. (15) and (16). Obviously, this approach does not involve any kind of approximation or assumption about the initial conditions.

B. Amplitude and phase equations

Substituting $\xi_k^\pm = \chi_k^\pm e^{i\phi_k^\pm}$ into Eq. (9), where $\chi_k^\pm$ and $\phi_k^\pm$ are the amplitude and the phase of the eigenmode, respectively, we get

$$\partial_t\left(\chi_k^\pm e^{i\phi_k^\pm}\right) + i\omega_k^\pm \chi_k^\pm e^{i\phi_k^\pm} = |N_{\xi k}^\pm|e^{i\phi_k^{N_{\xi\pm}}}, \tag{19}$$

where $|N_{\xi k}^\pm|e^{i\phi_k^{N_{\xi\pm}}}$ are the nonlinear terms given in Eq. (14), written in terms of their amplitudes and phases. Note that in order to obtain an explicit expression for $N_{\xi k}^\pm$ in terms of $\xi_k^\pm$, one would need to substitute Eqs. (15) and (16) into Eqs. (7) and (8), the result of which is then to be substituted into Eq. (14). See Sec. I C for the explicit calculation.

Taking the real part of Eq. (19), we obtain the amplitude equations

$$\left(\partial_t - \gamma_k^\pm\right)\chi_k^\pm = |N_{\xi k}^\pm|\cos\left(\phi_k^{N_{\xi\pm}} - \phi_k^\pm\right), \tag{20}$$

and taking the imaginary part and dividing by $\chi_k^\pm$, we get the phase equations

$$\partial_t \phi_k^\pm = -\omega_{kr}^\pm + \frac{|N_{\xi k}^\pm|}{\chi_k^\pm}\sin\left(\phi_k^{N_{\xi\pm}} - \phi_k^\pm\right). \tag{21}$$

The form of the amplitude equation, i.e. Eq. (20), means that the fixed point for the amplitude evolution is determined by the phase difference between $N_{\xi k}^{s_k}$ and $\xi_k^{s_k}$ for each s_k. However, such a fixed point keeps evolving since the phases themselves increase linearly with the linear frequency while being deformed by the nonlinear terms. Note that if the nonlinear phase is dominated by a slowly evolving mean phase (could be the case if the nonlinear interactions are dominated by the interactions with a zonal flow), the individual phases will be attracted to this nonlinear mean phase since if the individual phase is behind the nonlinear phase, the $\sin\left(\phi_k^{N_{\xi\pm}} - \phi_k^\pm\right)$ will be positive, causing the individual phase to accelerate, whereas if the individual phase is ahead of the nonlinear phase, it will be slowed down. However, since we have linear frequencies, it is impossible for individual phases to become phase locked directly with the slow nonlinear phase. Instead the nonlinear term plays a role akin to that of the ponderomotive force in parametric instability.

C. Nonlinear terms

In order to compute $N_{\xi k}^\pm$ in terms of $\xi_k^\pm$, we need to go back to Φ_k and n_k using Eqs. (15) and (16), compute the nonlinear terms (7) and (8) using those, and combine them as in Eq. (14). They can then be written in the form

$$N_{\xi k}^{s_k} = \frac{1}{2}\sum_\triangle \sum_{s_p, s_q} M_{\xi kpq}^{s_k s_p s_q} \xi_p^{s_p*} \xi_q^{s_q*} \tag{22}$$

in terms of the linear eigenmodes, where the sum over triangle notation indicates a sum over the wave-vectors p and q satisfying the triad interaction condition, and the sum over the signs s_p and s_q is over $s_p, s_q = \{(+,+),(+,-),(-,+),(-,-)\}$ for $s_k = (+,-)$, and the nonlinear interaction coefficients $M_{\xi kpq}^{s_k s_p s_q}$ in Eq. (22) can be written for interactions among non-zonal modes as

$$M_{\xi kpq}^{s_k s_p s_q} = m_{kpq}^{s_k s_p s_q}\left[q^2\left(B_q - i\Omega_q^{s_q*}\right) - p^2\left(B_p - i\Omega_p^{s_p*}\right)\right.$$
$$\left. -\left(q^2 - p^2\right)\left(B_k - i\Omega_k^{s_k}\right)\right], \tag{23}$$

where

$$m_{kpq}^{s_k s_p s_q} \equiv \frac{C\hat{\mathbf{z}} \times \mathbf{p} \cdot \mathbf{q}}{4\Omega_p^{s_p*}\Omega_q^{s_q*}q^2 p^2},$$

and $\Omega_k^\pm$ are defined in Eq. (10).

Note that these coefficients are complex and have different phases in general. In other words, the explicit forms of Eq. (21) can be written as

$$\partial_t \phi_k^{s_k} = -\omega_{kr}^{s_k} + \sum_\triangle \sum_{s_p, s_q} \frac{|M_{\xi kpq}^{s_k s_p s_q}||\xi_p^{s_p}||\xi_q^{s_q}|}{|\xi_k^{s_k}|}$$
$$\times \sin\left(\theta_{M_{\xi kpq}}^{s_k s_p s_q} - \phi_p^{s_p} - \phi_q^{s_q} - \phi_k^{s_k}\right), \tag{24}$$

where $\theta_{M_{\xi kpq}}^{s_k s_p s_q}$ is the phase of the nonlinear interaction coefficient $M_{\xi kpq}^{s_k s_p s_q}$.

II. INTERACTIONS AMONG DRIFT WAVES
A. Three wave interactions

Consider three separate modes k, p, and q that satisfy the triadic interaction condition $\mathbf{k} + \mathbf{p} + \mathbf{q} = 0$, possibly in the presence of other modes. The nonlinear term for the wave number k can then be divided into the interaction with the pair p and q, and the interaction with the rest of the modes (if they exist). If the three wave interaction that we consider is resonant, slightly off resonance, or completely non-resonant, its evolution is likely to be different, which can be considered as different scenarios. It may also be possible to model the effects of rest of the modes as background forcing, modification of the linear terms (à la eddy damping), or simply as stochastic noise. Thus, separating the nonlinear term into the interaction with the pair p and q (i.e., $N_{\xi kpq}^\pm$) and the interaction with the rest of the modes (i.e., $\delta N_{\xi kpq}^\pm$), we can write

$$\partial_t \xi_k^\pm + i\omega_k^\pm \xi_k^\pm = N_{\xi kpq}^\pm + \delta N_{\xi kpq}^\pm, \tag{25}$$

where

$$N_{\xi kpq}^\pm = M_{\xi kpq}^{\pm++}\xi_p^{+*}\xi_q^{+*} + M_{\xi kpq}^{\pm+-}\xi_p^{+*}\xi_q^{-*}$$
$$+ M_{\xi kpq}^{\pm-+}\xi_p^{-*}\xi_q^{+*} + M_{\xi kpq}^{\pm--}\xi_p^{-*}\xi_q^{-*},$$

with $M_{\xi kpq}^{\pm\pm\pm}$ being (complex) nonlinear interaction coefficients, and

$$\delta N_{\xi kpq}^\pm = N_{\xi k}^\pm - N_{\xi kpq}^\pm.$$

The p and q modes evolve similarly,

$$\partial_t \xi_p^\pm + i\omega_p^\pm \xi_p^\pm = N_{\xi pqk}^\pm + \delta N_{\xi pqk}^\pm, \tag{26}$$

$$\partial_t \xi_q^\pm + i\omega_q^\pm \xi_q^\pm = N_{\xi qkp}^\pm + \delta N_{\xi qkp}^\pm. \tag{27}$$

Notice that, since there are two eigenmodes, Eqs. (25)–(27) represent six equations. One can therefore consider resonances between three growing modes, two growing modes and a damped mode, or a growing mode and two damped modes, etc. However, since the frequencies are the same with opposing signs, and due to the condition that the flow field is real, we have both k_y and $-k_y$ components, whenever we have a resonance, for example, of the form $\omega_{\mathbf{k}}^+ + \omega_{\mathbf{p}}^+ + \omega_{\mathbf{q}}^+ = 0$ (with $\mathbf{k} + \mathbf{p} + \mathbf{q} = 0$), we also have $\omega_{\mathbf{k}}^- + \omega_{\mathbf{p}}^- + \omega_{\mathbf{q}}^- = 0$, $\omega_{\mathbf{k}}^+ - \omega_{-\mathbf{p}}^-$ $-\omega_{-\mathbf{q}}^- = 0$ or $\omega_{-\mathbf{k}}^- - \omega_{\mathbf{p}}^+ - \omega_{\mathbf{q}}^+ = 0$, etc. In other words, whenever we have a resonance for three + modes, we also have all the other combinations. The form of the resonance manifold can be seen in Figs. 1 and 2, for $C = 1$, $\kappa = 0.2$, and $\nu = D = 10^{-3}$, which we will refer to as the "$C = 1$ case."

The three wave interaction system (25)–(27) can be implemented numerically without much difficulty by dropping the δN_ξ terms above. One can also formulate the same three wave interaction problem in the original variables Φ_k, Φ_p, Φ_q, n_k, n_p, and n_q using the form (3) and (4) before the transformation and then transform the result using
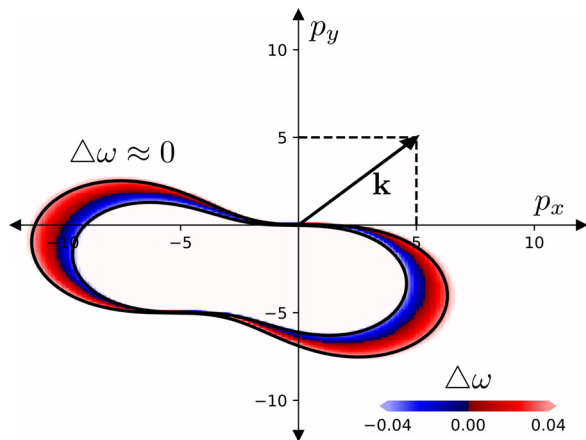
FIG. 1. The resonance manifold $\Delta\omega = \omega_{\mathbf{k}r}^+ + \omega_{\mathbf{p}r}^+ + \omega_{\mathbf{q}r}^+ = 0$ of the Hasegawa–Wakatani system for the case $C = 1.0$, $\kappa = 0.2$, $\nu = D = 10^{-3}$ is shown corresponding to the wave vector $\mathbf{k} = (5, 5)$ that is shown explicitly. Any $\mathbf{p}$ that falls onto the region inside the resonance manifold (shown here with a finite width of ± 0.04 with $\Delta\omega > 0$ in red and $\Delta\omega < 0$ in blue if in color) gives $\Delta\omega \approx 0$ (with $\mathbf{q} = -\mathbf{k} - \mathbf{p}$). As discussed in the text, because of the fact that the $(+)$ and $(-)$ modes have the same frequency (but opposite direction of propagation in y direction), all possible combinations of $(+)$ and $(-)$ modes resonate on the same manifold.

Eq. (13). Obviously, those two approaches are numerically equivalent and naturally they give exactly the same results. We used this to verify that the eigenmode computation was correct. While in general it is unclear if the eigenmode formulation provides any concrete advantage apart from diagonalizing the linear system, the advantage becomes self-evident if the resulting fluctuations have $\xi_{\mathbf{k}}^+ \gg \xi_{\mathbf{k}}^-$, and we can drop the $\xi_{\mathbf{k}}^-$ mode for example.

1. Is there a difference between exact and near resonances?

We first pick a primary wave-number $\mathbf{k} = (0, 1.125)$ which is the linearly most unstable mode on a grid with $dk_x = dk_y = 0.125$ for the $C = 1.0$ case and consider the resonance manifold as shown in Fig. 2(a) in order to pick a second wave-number $\mathbf{p} = (-0.5, -1.0)$ as the point on the k-space grid that is closest to the resonance manifold. The third wave-number $\mathbf{q}$ is computed from $\mathbf{k} + \mathbf{p} + \mathbf{q} = 0$. While a direct numerical simulation only has the wave-numbers on grid points, a three wave equation solver is not constrained to such a grid. We can instead compute $\mathbf{p}$ to be exactly on the resonance manifold—at least within some numerical precision—for example, by choosing $\mathbf{p} = (-0.5, -1.063\,232\,526\,549\,2)$. Solving the three wave equations numerically, using these slightly different sets of wave-numbers, we find that having exact resonance or near resonance (i.e., $\Delta\omega \approx 2 \times 10^{-15}$ vs $\Delta\omega \approx 0.01$) does not make much difference in terms of time evolution (see Fig. 3), while picking something like $\mathbf{p} = (-0.5, -1.5)$, which gives $\Delta\omega \approx 0.07$ (with $\omega_k \approx 0.1$ for comparison), gives a completely different time evolution, where one of the modes keeps growing linearly without being able to couple to the other two. We verified this for a bunch of different sets of wave numbers, and while there are some differences in detail, generally both exactly resonant or near resonant triads lead to saturation but non-resonant triads cannot saturate, possibly due to lack of efficient interactions. The boundary between what can be considered a near resonant vs non-resonant interaction can actually be defined using this criterion. In particular, it seems that the triads with one of the frequencies much smaller than the other two (i.e., $\omega_q \ll \omega_p \sim \omega_k$) tend to support larger overall $\Delta\omega$ and nonetheless reach saturation. However, it is not clear whether these observations from a single triad continue to hold when many triads are interacting with each other.
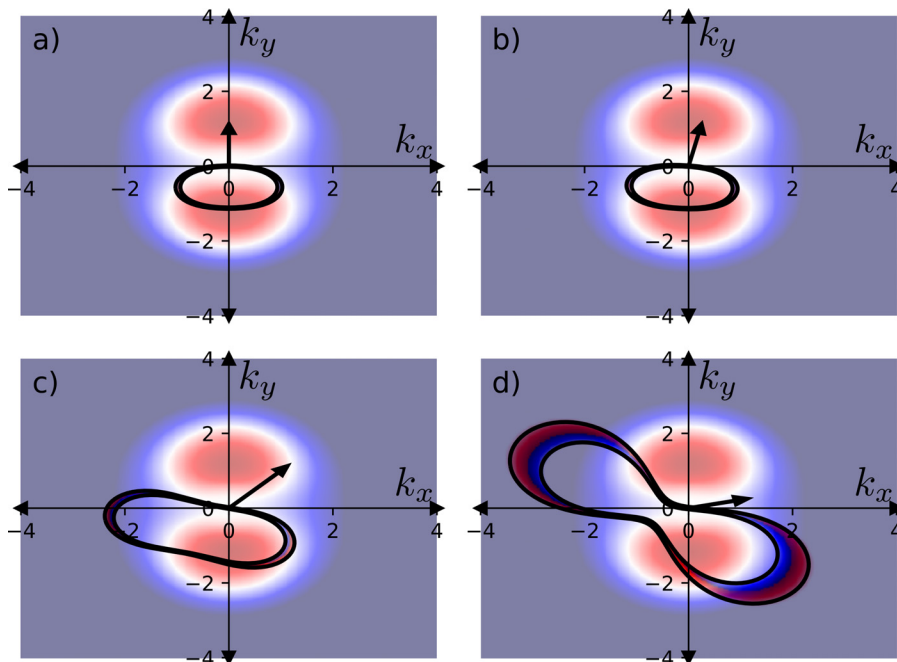

FIG. 2. The resonance manifold, shown on top of the growth rate where red corresponds to $\gamma_{\mathbf{k}}^+ > 0$ and blue to $\gamma_{\mathbf{k}}^+ < 0$ for (a) the most unstable model on the grid $\mathbf{k} = (0, 1.125)$, (b) a nearby mode with a small k_x component $\mathbf{k} = (0.250, 1.125)$, (c) a mode with $k_x = k_y$ that is $\mathbf{k} = (1.125, 1.125)$, and finally, (d) a mode that has $k_x \gg k_y$ with $\mathbf{k} = (1.125, 0.125)$.
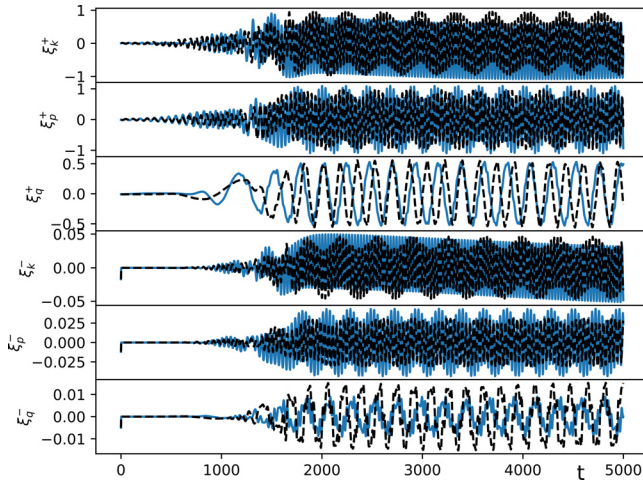
FIG. 3. Comparison between exact or near resonances, with real parts of each eigenmode shown for each wave number as labeled on the left side of the figure. The solid line is the exact (i.e., $\Delta\omega \approx 2 \times 10^{-15}$) resonance of $\mathbf{k} = (0, 1.125)$ with $\mathbf{p} = (-0.5, -1.063\,232\,526\,549\,2)$, whereas the dashed line is the near resonance with $\mathbf{p} = (-0.5, -1.0)$ and $\Delta\omega \approx 0.01$. While some details change, the overall behavior and saturation levels are actually very similar.

B. Phase evolution

Considering the (unwrapped) phase evolution of each of the modes of the near resonant triad with $\mathbf{k} = (0, 1.125)$ and $\mathbf{p} = (-0.5, -1.0)$, we observe that while some amplitude evolution continues, the phases converge toward straight lines, implying more or less constant frequencies in the final stage. These nonlinear frequencies are substantially shifted with respect to the initial linear frequencies

TABLE I. Saturated amplitudes, linear frequencies, linear growth rates, the final non-linear frequencies, and the $\delta\omega$'s that are computed from Eq. (28), rounded to two significant figures for the $C = 1$ case with $\mathbf{k} = (0, 1.125)$ and $\mathbf{p} = (-0.5, -1.0)$. Note that the basic assumption of Eq. (28) works only for linearly unstable modes, and for those, $\delta\omega$ is not far from $\omega_{nl} - \omega_r$.

	$k, +$	$p, +$	$q, +$	$k, -$	$p, -$	$q, -$
$\|\xi\|$	0.89	0.93	0.52	0.041	0.040	0.0017
ω_r	0.099	-0.088	-0.020	-0.099	0.088	0.020
γ	4.2×10^{-3}	3.1×10^{-3}	-1.8×10^{-4}	-1.8	-1.8	-4.8
ω_{nl}	0.20	-0.19	-0.016	0.20	-0.19	-0.016
$\delta\omega$	0.11	-0.11	$\cdots$	$\cdots$	$\cdots$	$\cdots$

due to the effect of nonlinear terms. However, it appears that the system remains in resonance as the sum of the final nonlinear frequencies remains very close to zero. In fact, it appears that the "near resonant" system evolves toward resonance as a result of these nonlinear corrections since $\Delta\omega$ decreases from the beginning toward the end.

Using Eqs. (20) and (21) with the assumption that $\partial_t \chi_k^\pm \approx 0$ and $\partial_t \phi_k^\pm = -\omega_{k,\mathrm{nl}}^\pm$ is a constant, we obtain the nonlinear frequency shift, i.e., $\delta\omega_{kr}^\pm = \omega_{k,\mathrm{nl}}^\pm - \omega_{kr}^\pm$ as

$$\delta\omega_{kr}^\pm = \mathrm{sign}(\omega_{kr})\sqrt{\frac{|N_{\bar\xi k}^\pm|^2}{|\xi_k^\pm|^2} - \gamma_k^{\pm 2}}, \qquad (28)$$

which can be computed given the final amplitudes and the nonlinear interaction coefficients (23). For example, for the case in Fig. 4, the smoothed saturated amplitudes are shown in Table I.

In order to elucidate dynamics of the phases in a triad, we define the sums of phases as a separate variable following Ref. 42,
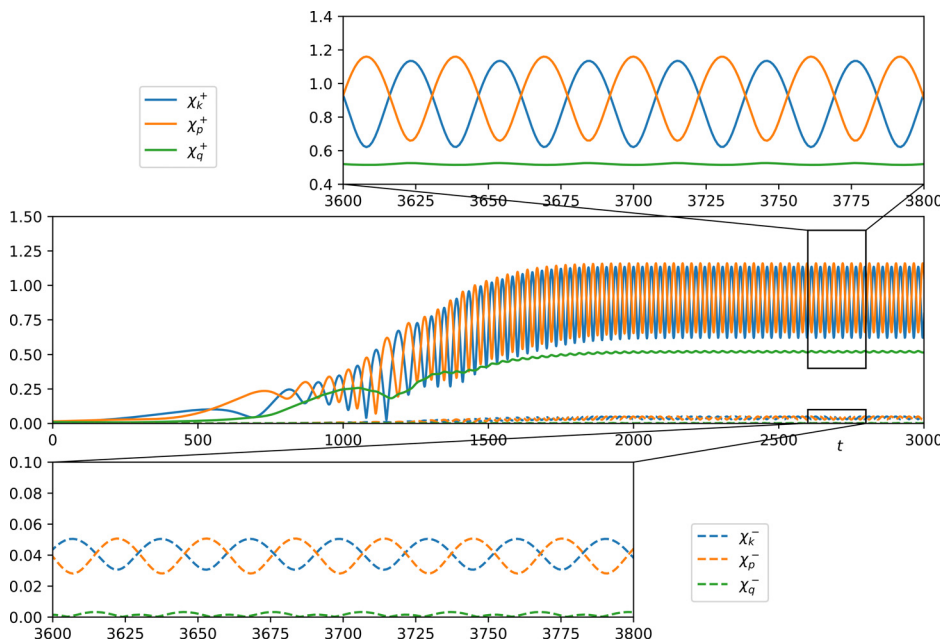

FIG. 4. Time evolution of the amplitudes of the eigenmodes for $C = 1$ case with $\mathbf{k} = (0, 1.125)$ and $\mathbf{p} = (-0.5, -1.0)$. We have a "saturated" state with oscillating amplitudes. It seems that as k and p (the two unstable modes and the two larger legs of the triads) exchange energy, q plays the role of the mediator.
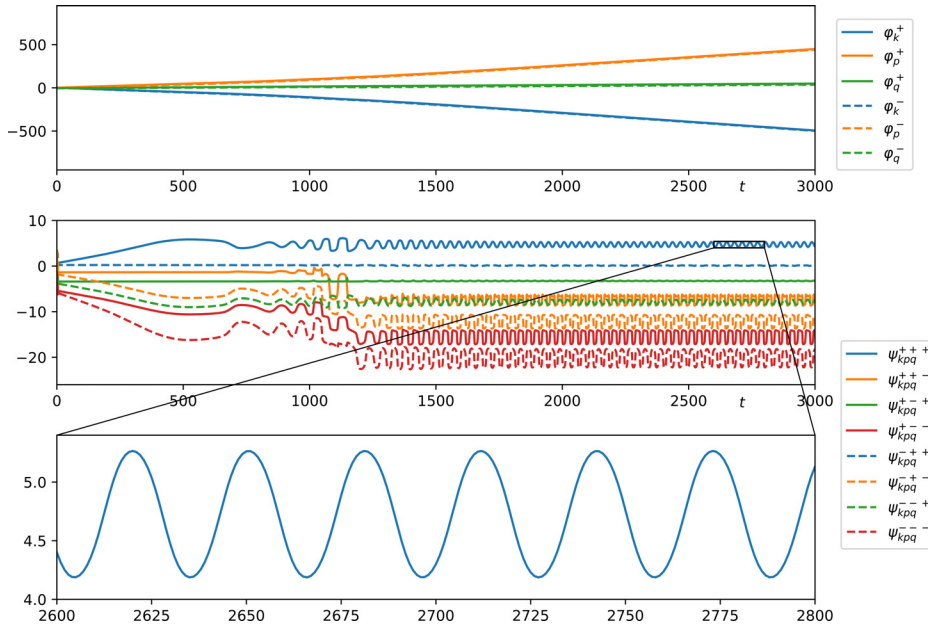
FIG. 5. Time evolution of the phases $\varphi_k^\pm$ and their sums $\psi_{kpq}^{s_p s_q s_k}$ for $C = 1$ case with $\mathbf{k} = (0, 1.125)$ and $\mathbf{p} = (-0.5, -1.0)$. Saturation of the amplitudes as seen in Fig. 4 is accompanied by a nonlinear frequency shift as shown in the top plot and the saturation of the $\psi_{kpq}^{s_p s_q s_k}$'s as shown in the bottom plot. Note that $\psi_{kpq}^{s_p s_q s_k}$ = const. would correspond to phase locking.

$$\psi_{kpq}^{s_k s_p s_q} \equiv \varphi_k^{s_k} + \varphi_p^{s_p} + \varphi_q^{s_q}. \tag{29}$$

We observe that while the phases keep increasing in time (see the top plot of Fig. 5 where the phases keep increasing linearly), for a steady state, the phase differences remain bounded (i.e., the bottom plot of Fig. 5, where the phase difference between three + modes oscillate between say, 4 and 5.5). Similarly, the frequencies, as computed by finite difference time derivatives of the phases, shown in Fig. 6, display bounded behavior, especially for those modes whose

amplitudes are significant. We can write the equations for the amplitudes as

$$\partial_t \chi_k^{s_k} - \gamma_k^{s_k} \chi_k^{s_k} = \sum_{\sigma_p, \sigma_q} m_{kpq}^{s_k \sigma_p \sigma_q} \cos\left(\delta_{kpq}^{s_k \sigma_p \sigma_q} - \psi_{kpq}^{s_k \sigma_p \sigma_q}\right) \chi_p^{\sigma_p} \chi_q^{\sigma_p}, \tag{30}$$

which contain the phases only through their sums (i.e., ψ variables). We can also write an equation for the $\psi_{kpq}^{s_k s_p s_q}$ explicitly as
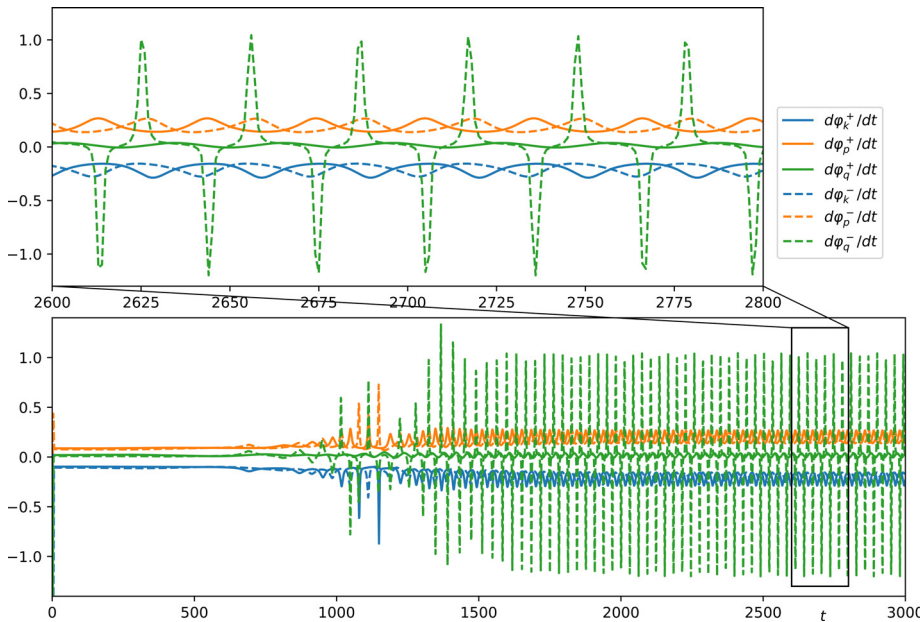

FIG. 6. Time derivatives of the phases $\varphi_k^\pm$ for $C = 1$ case with $\mathbf{k} = (0, 1.125)$ and $\mathbf{p} = (-0.5, -1.0)$, corresponding to nonlinear frequencies. Notice that while $d\varphi_q^-/dt$ appears to oscillate wildly, since its amplitude χ_q^- is vanishingly small, as can be seen in Fig. 4, these oscillations are not important for the rest of the dynamics.

$$\partial_t \psi_{kpq}^{s_k s_p s_q} + \left(\omega_k^{s_k} + \omega_p^{s_p} + \omega_p^{s_q} \right)$$

$$= \sum_{\sigma_p, \sigma_q} m_{kpq}^{s_k \sigma_p \sigma_q} \sin\left(\delta_{kpq}^{s_k \sigma_p \sigma_q} - \psi_{kpq}^{s_k \sigma_p \sigma_q} \right) \frac{\chi_p^{\sigma_p} \chi_q^{\sigma_q}}{\chi_k^{s_k}}$$

$$+ \sum_{\sigma_q, \sigma_k} m_{pqk}^{s_p \sigma_q \sigma_k} \sin\left(\delta_{pqk}^{s_p \sigma_q \sigma_k} - \psi_{pqk}^{s_p \sigma_q \sigma_k} \right) \frac{\chi_q^{\sigma_q} \chi_k^{\sigma_k}}{\chi_p^{s_p}}$$

$$+ \sum_{\sigma_k, \sigma_p} m_{qkp}^{s_q \sigma_k \sigma_p} \sin\left(\delta_{qkp}^{s_q \sigma_k \sigma_p} - \psi_{qkp}^{s_q \sigma_k \sigma_p} \right) \frac{\chi_k^{\sigma_k} \chi_p^{\sigma_p}}{\chi_q^{s_q}}. \quad (31)$$

While the form of Eq. (31) looks terribly complicated (e.g., when we expand the sums, we have eight equations, each of which has 12 terms on their right hand side), it is useful for getting an insight into phase locking. For example, by setting $\partial_t \psi_{kpq}^{s_k s_p s_q} = 0$ in Eq. (31), and $\partial_t \chi_k^{s_k} = 0$ in Eq. (30), we can obtain constant amplitude, phase locked solutions if such solutions exist. Unfortunately, even the computation of this "fixed point" requires numerical analysis. We can also integrate Eqs. (30) and (31) numerically, which gives exactly the same result as the system in terms of $\xi_k^{\pm}$.

III. INTERACTIONS WITH ZONAL FLOWS

When two non-zonal modes interact with a zonal one, the evolution equations and the nonlinear interaction coefficients are different from non-zonal three wave interactions discussed in Sec. II. Using the original variables Φ_k and n_k as in Eqs. (3) and (4), zonal and non-zonal modes interact with the same nonlinear interaction coefficients but different linear propagators. However, when we diagonalize the linear propagator, the nonlinear interaction coefficients for zonal and non-zonal modes differentiate.

In particular, we have

$$M_{kpq}^{\phi s_p s_q} = -\frac{\hat{\mathbf{z}} \times \mathbf{p} \cdot \mathbf{q} (q^2 - p^2) C^2}{4 \Omega_p^{s_p *} \Omega_q^{s_q *} k^2 p^2 q^2}, \quad (32)$$

$$M_{kpq}^{n s_p s_q} = \frac{\hat{\mathbf{z}} \times \mathbf{p} \cdot \mathbf{q} C}{4 \Omega_p^{s_p *} \Omega_q^{s_q *} p^2 q^2} \left[\left(B_q - i\Omega_q^{s_q *} \right) q^2 - \left(B_p - i\Omega_p^{s_p *} \right) p^2 \right], \quad (33)$$

$$M_{kpq}^{s_k \phi s_q} = i \frac{\hat{\mathbf{z}} \times \mathbf{p} \cdot \mathbf{q}}{2 \Omega_q^{s_q *} q^2} \left[\left(B_q - i\Omega_q^{s_q *} \right) q^2 - \left(B_k - i\Omega_k^{s_k} \right) \left(q^2 - p^2 \right) \right], \quad (34)$$

$$M_{kpq}^{s_k n s_q} = i \frac{\hat{\mathbf{z}} \times \mathbf{p} \cdot \mathbf{q} C}{2 \Omega_q^{s_q *} q^2}, \quad (35)$$

so that for three waves k, p, and q with $q_y = 0$, we can write

$$\partial_t \bar{\Phi}_q + \nu_{ZF} \bar{\Phi}_q = \sum_{s_k, s_p} M_{qkp}^{\phi s_k s_p} \xi_k^{s_k *} \xi_p^{s_p *}, \quad (36)$$

$$\partial_t \bar{n}_q + D_{ZF} \bar{n}_q = \sum_{s_k, s_p} M_{qkp}^{n s_k s_p} \xi_k^{s_k *} \xi_p^{s_p *}, \quad (37)$$

$$\partial_t \xi_k^{s_k} + i\omega_k^{s_k} \xi_k^{s_k} = \sum_{s_p} M_{kpq}^{s_k s_p \phi} \xi_p^{s_p *} \Phi_q^* + M_{kpq}^{s_k s_p n} \xi_p^{s_p *} n_q^*, \quad (38)$$

$$\partial_t \xi_p^{s_p} + i\omega_p^{s_p} \xi_p^{s_p} = \sum_{s_p} M_{pqk}^{s_p \phi s_k} \Phi_q^* \xi_k^{s_k *} + M_{pqk}^{s_p n s_k} n_q^* \xi_k^{s_k *}. \quad (39)$$

We can write these in the form (25)–(27) by letting $\xi_q^+ = \Phi_q$ and $\xi_q^- = n_q$ and paying attention to the form of the interaction coefficient $M_{\xi kpq}^{s_k s_p s_q}$ when one of the legs is zonal.

In order to study the interactions between two modes with a zonal flow in the Hasegawa–Wakatani system numerically, we pick a primary wave-number $\mathbf{k} = (0, 1.125)$ which is the linearly most unstable mode on a grid with $dk_x = dk_y = 0.125$ for the $C = 1.0$ case. We choose $\mathbf{p} = (-0.5, -1.125)$ so that $\mathbf{q} = (0.5, 0)$ is a zonal wave number. The 6 field variables are now $\xi_k^{\pm}$, $\xi_p^{\pm}$, Φ_q, and n_q whose evolutions are shown in Fig. 7 for the case $C = 1$, $\nu_Z = D_Z = 0$, and $\gamma_k \gtrsim \gamma_p > 0$. In the final state, the system finds a fixed point characterized by constant nonlinear frequency shifts, constant amplitudes, and constant ψ_{kpq}'s. However, this kind of steady state solution seems to be exclusive to the single triad case.

A. Triad pairs

Because of the symmetry of the system, if we consider two wave-numbers $\mathbf{p}_1 = -\mathbf{k} - \mathbf{q}$ and $\mathbf{p}_2 = -\mathbf{k} + \mathbf{q}$ with $\mathbf{k}$ in $\hat{\mathbf{y}}$ and $\mathbf{q}$ in $\hat{\mathbf{x}}$ directions, we get two triads that are reflections of one another with respect to the axis defined by $\mathbf{k}$. Such a system involves four different wave-numbers connected with two different triads. Including the $p \rightleftarrows q$ transformation, we have four triads as shown in Fig. 8. However, as long as we use symmetric forms for the interaction coefficients, we can drop the two triads we obtain from the $p \rightleftarrows q$ transformation and count only two triads. Since the two triads of such a pair are reflections of one another, the nonlinear interaction coefficients differ only in sign while the complex frequencies are the same, and as there are two eigenmodes for each wave-number, we have eight equations. The equations for zonal modes can be written from Eqs. (36) and (37) as

$$\partial_t \Phi_q + \nu_Z \Phi_q = \sum_{s_k, s_p} M_{qkp_1}^{\phi s_k s_p} \left(\xi_k^{s_k *} \xi_{p_1}^{s_p *} - \xi_k^{s_k} \xi_{p_2}^{s_p} \right), \quad (40)$$

$$\partial_t n_q + D_Z n_q = \sum_{s_k, s_p} M_{qkp}^{n s_k s_p} \left(\xi_k^{s_k *} \xi_{p_1}^{s_p *} - \xi_k^{s_k} \xi_{p_2}^{s_p} \right), \quad (41)$$

which is possible since $M_{\xi kp_2 q}^{s_k s_p \{n, \phi\}} = -M_{\xi kp_1 q}^{s_k s_p \{n, \phi\}}$ because $p_2^2 = p_1^2$ and $p_{2y} = p_{1y}$ while $p_{2x} = -p_{2x}$. The equation for the primary mode can be written as

$$\partial_t \xi_k^{s_k} + i\omega_k^{s_k} \xi_k^{s_k} = \sum_{s_p} \left[M_{\xi kpq}^{s_k s_p \phi} \left(\Phi_q^* \xi_{p_1}^{s_p *} + \Phi_q \xi_{p_2}^{s_p *} \right) \right.$$
$$\left. + M_{\xi kpq}^{s_k s_p n} \left(n_q^* \xi_{p_1}^{s_p *} + n_q \xi_{p_2}^{s_p *} \right) \right], \quad (42)$$

and the remaining two equations are the same as (39) but with different signs and conjugations,

$$\partial_t \xi_{p_1}^{s_p} + i\omega_{p_1}^{s_p} \xi_{p_1}^{s_p} = \sum_{s_k} \left(M_{\xi p_1 kq}^{s_p s_k \phi} \Phi_q^* + M_{\xi p_1 kq}^{s_p s_k n} n_q^* \right) \xi_k^{s_k *}, \quad (43)$$

$$\partial_t \xi_{p_2}^{s_p} + i\omega_{p_2}^{s_p} \xi_{p_2}^{s_p} = -\sum_{s_k} \left(M_{\xi p_1 kq}^{s_p s_k \phi} \Phi_q + M_{\xi p_1 kq}^{s_p s_k n} n_q \right) \xi_k^{s_k *}, \quad (44)$$

where $\omega_{p_2}^{s_p} = \omega_{p_1}^{s_p}$. Notice that this is also equivalent to one of the radial Fourier modes of a quasi-linear (e.g., zonostrophic) interaction, where for each field one would consider a single p_y but the full spatial dependence in x.

The results of the system (40) and (44) are shown in Fig. 9 for the $C = 1$ case with $k_y = 1.125$ [i.e., $\mathbf{k} = (0, k_y)$, $\mathbf{p}_1 = (-q, -k_y)$, $\mathbf{p}_2 = (q, -k_y)$, and $\mathbf{q} = (q, 0)$] for $q = (1.0, 1.5, 2.0, 4.0)$ from top to
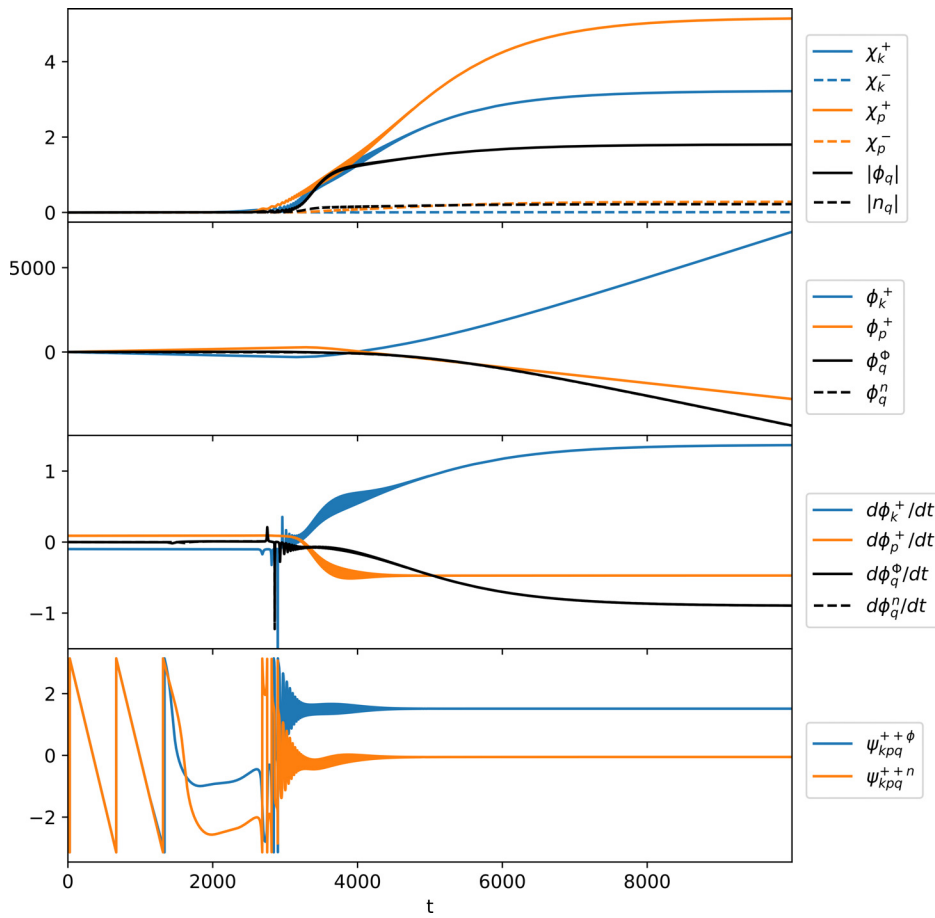
FIG. 7. Time evolution of the three wave equations involving a zonal mode q, for the case $C = 1$, $\nu_Z = D_Z = 0$, and $\gamma_k \gtrsim \gamma_p > 0$ with $k_y = 1.125$ and $q = 0.5$ [i.e., $\mathbf{k} = (0, k_y)$, $\mathbf{p} = (-q, -k_y)$ and $\mathbf{q} = (q, 0)$]. The system reaches a steady state by introducing nonlinear frequencies in order to arrive at a state where the sums of phases ψ_{kpq}'s are constant. Note that it is p which becomes the dominant mode in the final state and the existence of zonal flows does not lead to a complete suppression of turbulence. Instead the zonal flow acquires a constant nonlinear frequency.
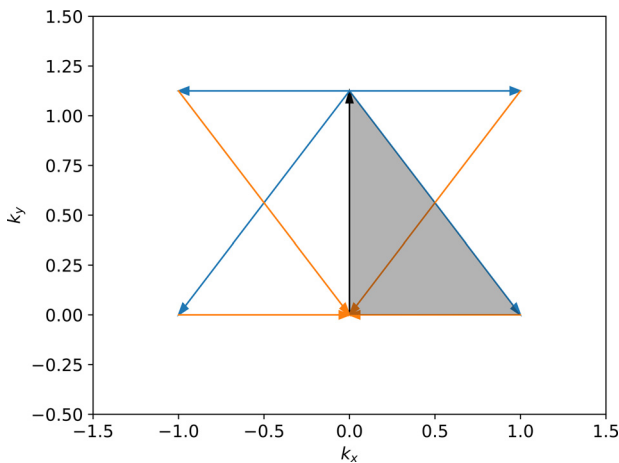

FIG. 8. All the four triads involved in the interaction between the most unstable mode with $\mathbf{k} = k_y \hat{\mathbf{y}}$ with $k_y = 1.125$ and a given zonal mode with $q = 1.0$, obtained by reflection with respect to $\mathbf{k}$ and the exchange of p and q of the primary triad, which is shaded. The existence of the reflected triad is indeed important as it changes the qualitative behavior with respect to the single triad case.

bottom, respectively. For $q \leq k_y$, we have instability and p keeps growing exponentially whereas for $q > k_y$, we get some sort of steady or limit cycle state. Performing a scan of k_y and q for this two triad system (keeping in mind that for $k_y > 2$ we have no instability and therefore the pump mode decays), we observe that we can define a four wave interaction condition of the form $\omega_{kr}^{s_k} + \omega_{p1r}^{s_{p1}} + \omega_{p2r}^{s_{p2}} + \omega_{qr}^{s_q} = 0$, which turns into $\Omega_k^{s_k} + 2\Omega_p^{s_p} = 0$ since $\omega_{qr} = 0$ and $\omega_{p1r} = \omega_{p2r} = \omega_{pr}$. During our studies, we have observed three distinct regions: for $q < 1$, the ξ_p^+ modes grow exponentially as in the top plot of Fig. 9, for $q \approx 1$, we have saturation and then somewhat chaotic evolution as in the second plot of Fig. 9, and finally for $q \gg 1$, we observe limit cycle oscillations between ξ_k^+ and ξ_p^+ modes, mediated by zonal flows as in the bottom plot of Fig. 9.

One is tempted to argue that since the p with $p_x < p_y$ wins the competition to attract more energy, the cascade will proceed in this direction, and in the next step, we can consider the interaction of this ξ_p^+ as the pump mode for the next triad, etc. However, since each mode interacts with many triads simultaneously, the fact that ξ_p^+ wins the competition in the single triad (or one triad and its reflection) configuration does not really mean the energy will indeed go this way.
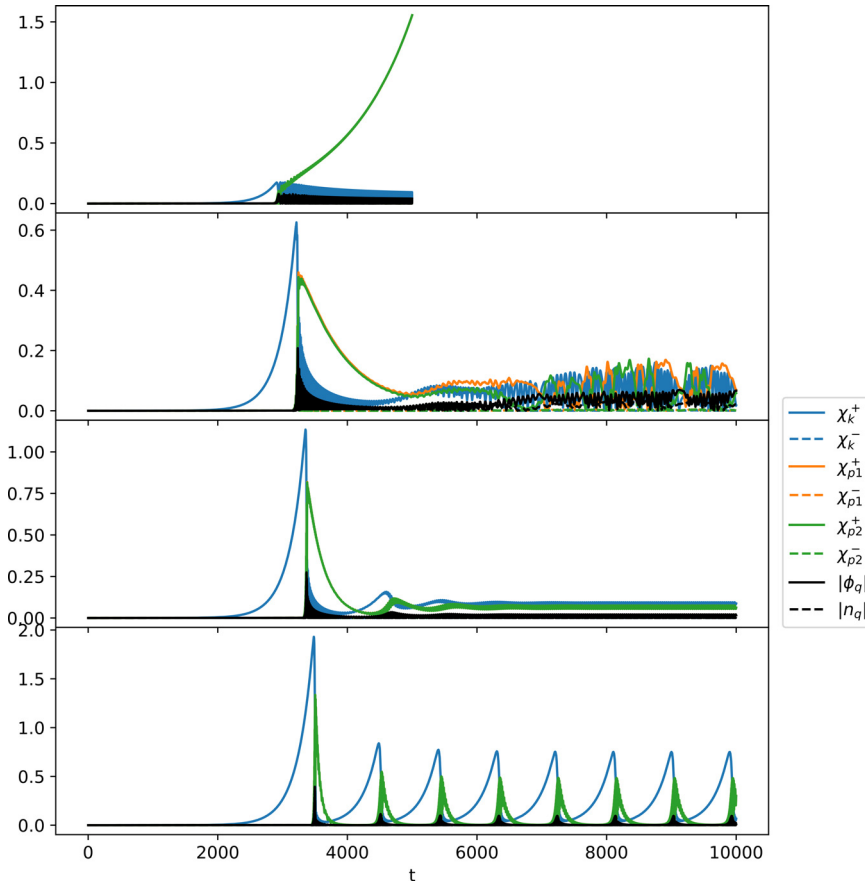
FIG. 9. Evolution of a triad pair with the same parameters as Fig. 7, no zonal flow damping $\nu_Z = D_Z = 0$ and $k_y = 1.125$ [i.e., $\mathbf{k} = (0, k_y)$, $\mathbf{p}_1 = (-q, -k_y)$, $\mathbf{p}_1 = (q, -k_y)$, $\mathbf{p}_2 = (q, -k_y)$ and $\mathbf{q} = (q, 0)$] for four different values of $q = (1.0, 1.5, 2.0,$ and $4.0)$ from top to bottom for which the growth rates of the subdominant modes are $\gamma_p = (0.00099, -0.0016, -0.0042,$ and $-0.017)$, respectively. Note that apart from the second plot, which displays some chaotic behavior, the curves for $\xi_{p_1}^+$ and $\xi_{p_2}^+$ overlap almost exactly.

B. Triad networks

In order to study the fate of the cascade, we need to consider multiple triads that are connected to one another. However, as we add more zonal and non-zonal modes, it becomes quite complicated to keep track of all the interaction coefficients, conjugations, etc. In order to simplify this task, we can divide the problem into two steps: (i) construction of a network of three body interactions and (ii) computation of the evolution of the field variables on this network. For example, for the above problem, we need to consider a network of $N_k = 4$ wave number nodes, coupled to $N_t = 2$ triads, with $N_f = 2$ fields in each node, with an interaction coefficient of the size $N_f \times N_f \times N_f$ for each connection. Since a network in Fourier space is made up of three body interactions, for each node, we can compute a list of interacting pairs and the interaction coefficients, so that we can write

$$\partial_t \xi_\ell^i + L_\ell^{ij} \xi_\ell^j = \frac{1}{2N} \sum_{\ell', \ell'' = \mathbf{i}_\ell} M_{\ell\ell'\ell''}^{ijk} \left(\xi_{\ell'}^j\right)^{c_{\ell'}} \left(\xi_{\ell''}^k\right)^{c_{\ell''}}, \quad (45)$$

where $\mathbf{i}_\ell$ is the list of precomputed interaction pairs for the node ℓ. The indices $i, j,$ and k correspond to different fields (eigenmodes or Φ_k and n_k), the matrix L_ℓ^{ij} is the linear matrix in k space (i.e., diagonal with the elements $i\omega_\ell^\pm$ for the eigenmodes), the $M_{\ell\ell'\ell''}^{ijk}$ is the interaction coefficient for each interaction, and N is the number of independent wave number nodes so that when we reach the full grid, we have

exactly the same interaction coefficients as the system formulated using discrete fast Fourier transforms (i.e., divided by $N_x \times N_y$). Finally, if we write the triad interaction condition in the form $\mathbf{k}_\ell + \sigma_{\ell'} \mathbf{k}_{\ell'} + \sigma_{\ell''} \mathbf{k}_{\ell''} = 0$, where σ are ± 1, the $(\xi_\ell^j)^{c_{\ell'}}$ are defined as

$$\left(\xi_{\ell'}^j\right)^{c_{\ell'}} = \begin{cases} \xi_{\ell'}^j & \sigma_{\ell'} = -1, \\ \xi_{\ell'}^{j*} & \sigma_{\ell'} = +1. \end{cases}$$

This is necessary unless we have the negative of each wave number vector as a separate node in the network.

Notice that when computing the nonlinear interaction coefficients for the eigenmodes, we would use (23) if all the nodes have nonzero k_y. In contrast, we would use Eqs. (32) and (33) if the receiving node (i.e., node ℓ) is zonal or Eqs. (34) and (35) if one of the interacting pairs (i.e., ℓ' or ℓ'') is zonal. Two or more zonal modes do not interact because of the geometric factor $\hat{\mathbf{z}} \times \mathbf{p} \cdot \mathbf{q}$, which appears in front of all the interaction coefficients.

Finally, if it makes sense to zero out some of the fields at a given wave-number (e.g., in eigenmode formulation, we may decide to throw away some damped modes), one may switch to a formulation where each node corresponds to a wave-number/field variable combination via $\{k_x, k_y, s_k\} \rightarrow \ell$. In this case, assuming that the linear matrix L_ℓ^{ij} in Eq. (45) diagonal takes the form

$$\partial_t \xi_\ell + i\omega_\ell \xi_\ell = \frac{1}{N} \sum_{\ell',\ell''=\mathbf{i}_\ell} M_{\ell\ell'\ell''} \xi_{\ell'}^{c_{\ell'}} \xi_{\ell''}^{c_{\ell''}}. \tag{46}$$

C. Order parameters

The phases of wave-number nodes in Hasegawa–Wakatani turbulence evolve according to Eq. (21) or written explicitly as Eq. (24). This suggests that one can possibly define some kind of order parameter for this system. The usual definition of the Kuramoto order parameter can be written for the network formulation of Eq. (46) as

$$z = r e^{i\psi} = \frac{1}{N} \sum_\ell e^{i\varphi_\ell}, \tag{47}$$

without explicitly distinguishing $+$ or $-$ modes. However, this order parameter based on an unweighted sum is probably relevant only if all the oscillators were identical with all-to-all, unweighted couplings of the Kuramoto type. Instead we can use an amplitude filtered Kuramoto order parameter (i.e., the sum is computed only over the oscillators with an amplitude larger than a threshold) or define a weighted version of Eq. (47) as

$$z = r e^{i\psi} = \frac{\sum_\ell \chi_\ell e^{i\varphi_\ell}}{\sum_\ell \chi_\ell}, \tag{48}$$

whose absolute value would tends toward 1 if the relevant phases (i.e., those that have large amplitude) are the same. However, note that the weighted order parameter tends toward 1 also when one of the modes dominates over the others, while ψ as defined in Eq. (48) can still be used as a mean phase.

It would also make sense to look at the net effect on the nonlinear term on the phases instead. As discussed in Sec. I B, since we can write

$$\partial_t \varphi_\ell = -\omega_\ell + \frac{1}{N\chi_\ell} \text{Im} \left[\sum_{\ell',\ell''=\mathbf{i}_\ell} M_{\ell\ell'\ell''} \xi_{\ell'}^{c_{\ell'}} \xi_{\ell''}^{c_{\ell''}} e^{-i\varphi_\ell} \right], \tag{49}$$

for the evolution of the phase, we can define

$$Z_\ell = R_\ell e^{i\psi_\ell} = \frac{1}{N\chi_\ell} \left(\sum_{\ell',\ell''=\mathbf{i}_\ell} M_{\ell\ell'\ell''} \xi_{\ell'}^{c_{\ell'}} \xi_{\ell''}^{c_{\ell''}} \right), \tag{50}$$

with d_ℓ being the number of interactions for the node ℓ (i.e., length of $\mathbf{i}_\ell$), as some kind of local order parameter for the node ℓ, allowing us to write the phase equation as

$$\partial_t \varphi_\ell = -\omega_\ell + R_\ell \sin(\psi_\ell - \varphi_\ell), \tag{51}$$

which attracts the system toward $\varphi_\ell = \psi_\ell + 2n\pi$.

D. Specific network configurations

In this section, we implement the solver for Eq. (45) in a generic network formulation and report the results in a number of specific network configurations. The ode solver is written in python and uses a standard adaptive time step Runge–Kutta 4/5 algorithm. While we did not perform extensive numerical tests, the results that we report below are consistently robust from a numerical point of view.

1. Network with a single k_y

We consider a network of triad pairs as discussed in Sec. III A with a single value of k_y and multiple q values that go from 0.125 to 4.0 in steps of 0.125. Notice that such a network has many different types of interactions as shown in Fig. 10, but all of those involve one of the zonal modes, which means that if we compute the inverse Fourier transform in the x direction, the network can be seen to be equivalent to the single k_y, full-x, quasi-linear model[43,44] since in both cases we have full spatial evolution in x direction but the only nonlinear coupling is with the zonal flow.

For the case $C = 1$, without zonal flow damping (not shown), we observe that the zonal flows dominate, and all the other modes decay to zero. This may well be what happens also in direct numerical simulations (DNS) eventually: what we observe in numerical simulations without zonal flow damping is a continual increase in zonal flows even for very long simulations.

In contrast, when we introduce zonal flow damping by letting $\nu_{ZF} = D_{ZF} = 10^{-3}$, we get dynamics and k-spectra which look more like fully developed Hasegawa-Wakatani turbulence, as shown in Figure 11, with high levels of zonal flows at large scales.

The order parameters, as defined in Eq. (47) or (48), are shown for this case in Fig. 12, which do not display a clear sign of synchronization.

2. Network with a single q

Here, we consider a network of triad pairs with a single q and a grid of values of k_y going from 0.125 to 4.0 in steps of 0.125. A reduced version of such a network is shown in Figure 13. Physically this network corresponds to the opposite case where we consider a single q
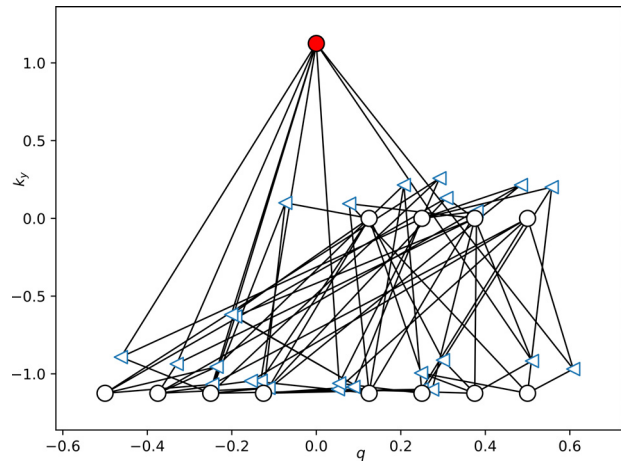

FIG. 10. The structure of the network with a single k_y with $k_y = 1.125$ shown as a filled (red if in color) node. Here, each circle represents a node (i.e., a wave-number with the same k_y but different $k_x = \pm q$), and each triangle represents a triad (i.e., three body) interaction among the nodes to which it is connected. Since the wave-numbers only interact through triad interactions, each-node is connected to a triad, and each triad is connected to three nodes (denoting the interacting wavenumbers). A reduced version with q values that only go up to 0.5 is shown for clarity. Notice that in this network while all of the 26 triads involve one of the zonal modes, only 8 of them involve the $q = 0$ mode.
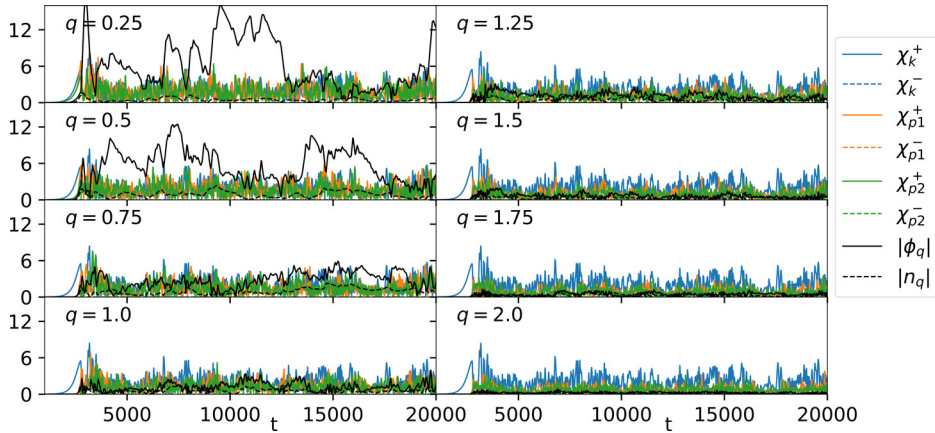
FIG. 11. Time evolution for a number of triad pairs (as defined in Sec. III A) for a single k_y but with different values of q in the network of interacting triads for $C = 1$ case with $\nu_{ZF} = D_{ZF} = 10^{-3}$. Note that the different plots show different q values in a single run. Here we observe a steady state turbulence level, with zonal flows (i.e., $|\Phi_q|$) dominating at large scales (e.g., $q = 0.25$ and $q = 0.5$).

with the whole y dynamics if we compute the inverse Fourier transform in y. Since it involves bunch of oscillators with different frequencies (as ω is mostly a function of k_y) that are coupled to each other and to a zonal mode that may play the role of a dominant mean field, it has the basic ingredients that may lead to synchronization.

Nonetheless numerical observations suggest that there is no obvious route to global synchronization in the three body network of interacting triads consisting of a zonal mode and drift waves of different k_y either. The weighted order parameter shows a brief increase during the nonlinear saturation phase as the energy is transferred to the zonal flow, but otherwise it remains close to zero, while the Kuramoto order parameter simply remains close to zero the whole time as can be seen in Fig. 14. Since we observed no qualitative difference between the runs with or without zonal flow damping for this case, we only show those with $\nu_{ZF} = D_{ZF} = 10^{-3}$.
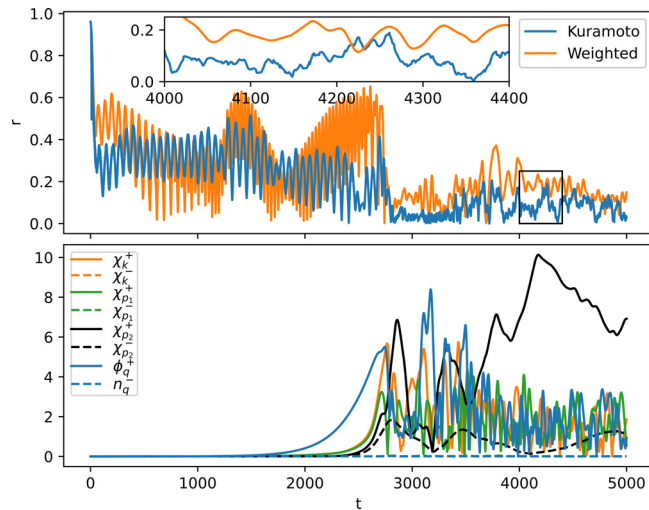
E. Direct numerical simulations

One can think of direct numerical simulation (DNS) on a regular rectangular grid as a "network" in Fourier space, in the sense that it consists of a collection of wave number nodes connected to each other through triadic interactions. In contrast to the networks that we considered that contain a single zonal mode, or a single $q = 0$ mode, a regular rectangular grid has all the possible wave-numbers in a particular range, and it allows using more efficient methods for computing the convolution sums. In practice, the high resolution direct numerical simulations that we discuss here were performed with a standard pseudo-spectral solver (i.e., with periodic boundary conditions in both directions) using 2/3 rule for dealiasing and adaptive time stepping.
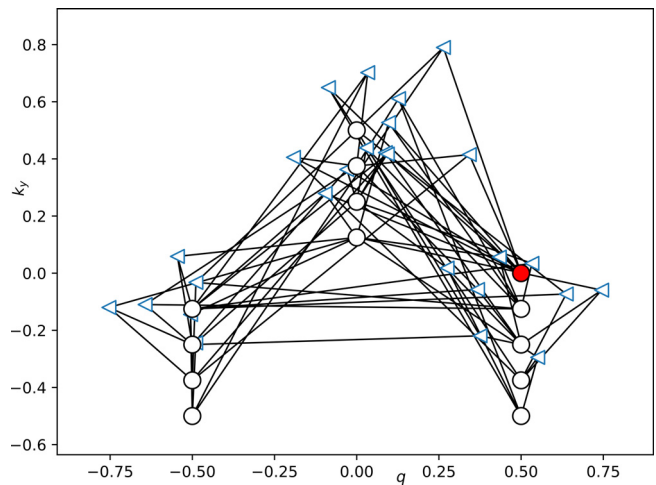

FIG. 12. The top plot shows the order parameter r defined in Eqs. (47) or (48) as a function of time for a network with single k_y and multiple q, while the bottom plot is the same as the $q = 0.5$ plot of Fig. 11, shown here for reference only up to $t = 5000$. The two definitions of the order parameter seem to be in reasonable agreement, maybe apart from the initial linear growth phase.

FIG. 13. The structure of the network with a single $q = 0.5$ zonal mode, shown as a filled (red if in color) node (also see Fig. 10). Here, each circle represents a node (i.e., a wave-number with the same $k_x = q$ but different k_y), and each triangle represents a triad (i.e., three body) interaction among the nodes to which it is connected. Since the wave-numbers only interact through triad interactions, each-node is connected to a triad, and each triad is connected to three nodes (denoting the interacting wavenumbers). A reduced version with k_y values that only go up to 0.5 is shown for clarity. Note that only 8 of the full 26 triads that are shown involve the zonal flow.
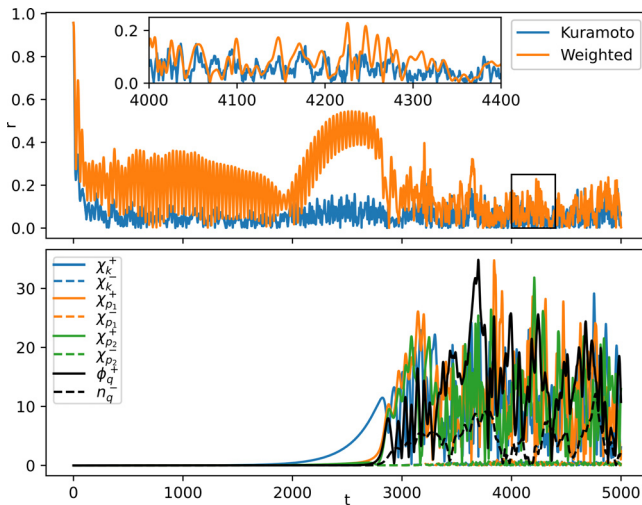
FIG. 14. The top plot shows the order parameter r defined in Eqs. (47) or (48) as a function of time for a network with single q and multiple k_y, while the bottom plot shows the amplitudes of a triad pair with $q = 0.5$ and $k_y = 1.125$, within such a network. The two definitions of the order parameter are in reasonable agreement apart from the peak around $t = 2500$ for the weighted order parameter, which corresponds to the linear growth phase, where only a few modes around the most unstable mode dominate. This can be seen at the bottom plot where the blue curve clearly dominates around $t = 2500$.

As with all the previous examples of single or multiple triads, or networks with a particular selection of nodes and triads, we use $C = 1$, $\kappa = 0.2$. Since we have a larger range of wave-numbers, we choose $\nu = D = 10^{-4}$, with a box size of $L_x = L_y = 16\pi$ and a padded resolution of 1024×1024. The results show (see Figs. 15 and 16) the following:

(i) Initial linear growth followed by nonlinear saturation.
(ii) Formation and finally suppression of nonlinear convective cells that transfer vorticity radially.
(iii) Consequent stratification of vorticity leading to a state dominated by zonal flows (as in Fig. 16).
(iv) Coherent nonlinear structures (e.g., vortices) that are advected by the zonal flows in regions of weak zonal shear
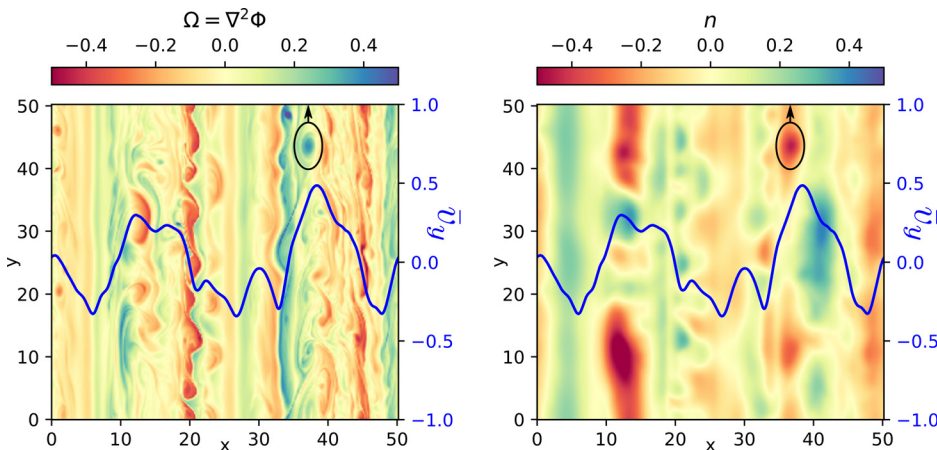

FIG. 15. The top plot shows the order parameter r defined in Eqs. (47) or (48) as a function of time for a DNS. The bottom plot shows the amplitudes of a triad pair with $q = 0.5$ and $k_y = 1.125$ in order to compare with the earlier plots. The saturation levels for the amplitudes are different because of the normalization factor $N_x^{-1} N_y^{-1}$ in front of the nonlinear term implied in discrete Fourier transforms.

get sheared apart if they fall into a region of strong zonal shear.

Since the wave-like dynamics seems to be primarily in y direction and reasonably localized in x, we can compute the Fourier transform in y and plot phase of $\xi_{k_y}^{\pm} = \chi_{k_y}^{\pm} e^{i\phi_{k_y}^{\pm}}$ at each x and compute $\partial_t \phi_{k_y}^{\pm}(x, t)$ in order to compute the phase speeds (see Fig. 17). We can also compute an order parameter as a function of x and t from these data.

While it is clear from Fig. 15 that there is no global synchronization in direct numerical simulations, the plateau form of the phase velocity as a function of k_y at the radii where it is positive for large scales suggests that a process of phase locking similar to soliton formation in nonlinear Schrödinger equation, where nonlinearity would balance dispersion, is at play for a range of k_y values around the linearly unstable mode, while ω/k_y being the same across a range of x and k_y values is obviously very different from ω being the same. However, if we note that the nonlinear dispersion relation takes the form $\omega(x, k_y) = \bar{v}_\phi(x)k_y$, at the lowest order we can see that the frequency in the frame moving with the zonal flow velocity becomes zero. This is

FIG. 16. Snapshots of vorticity and density at $t = 5000$ from DNS. The blue curve in both plots shows the zonal velocity whose values are given on the right hand axes. An example is coherent vortex. The one that was moving upwards is encircled.
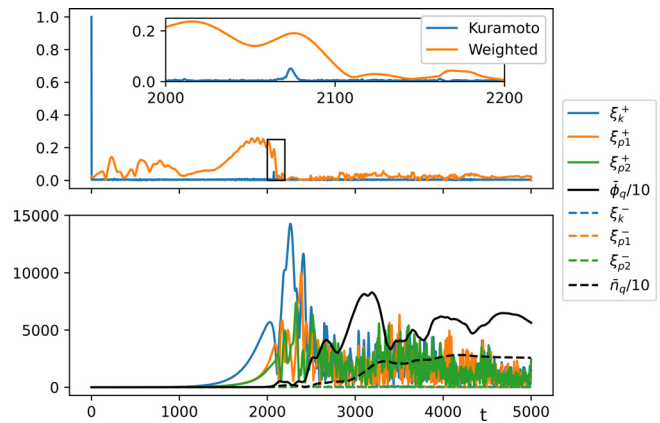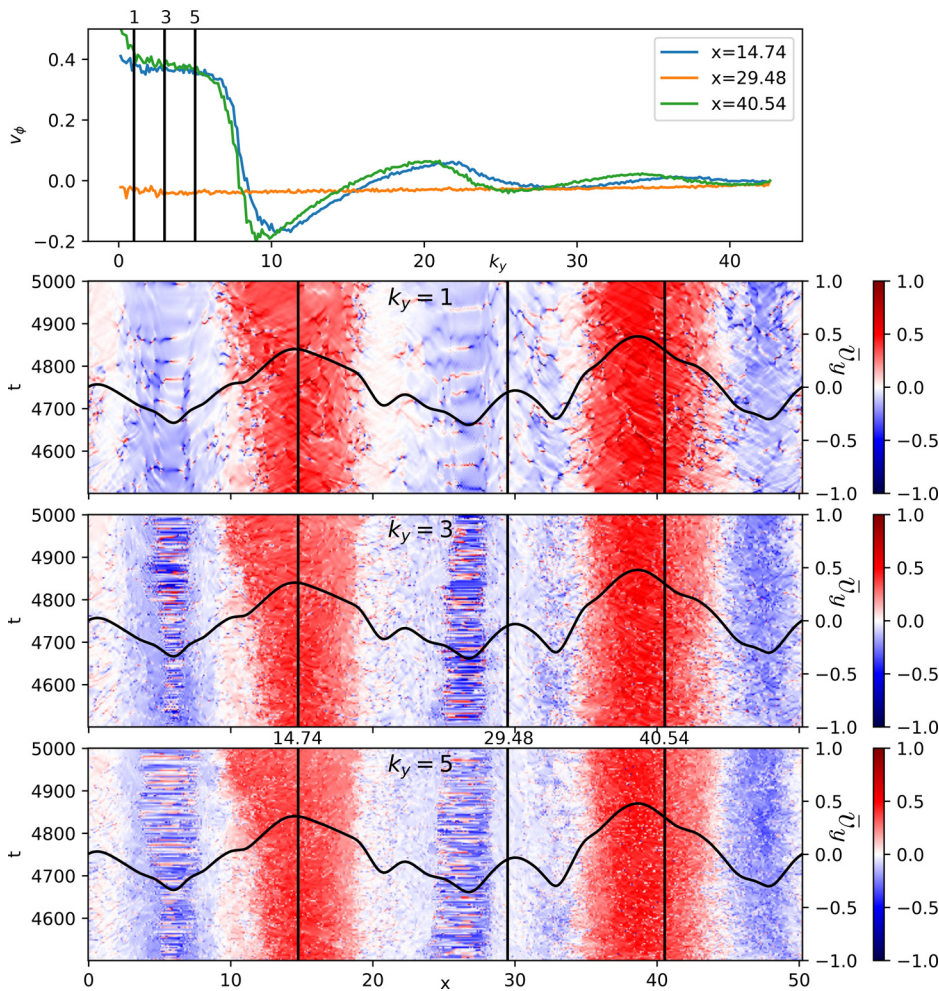
FIG. 17. Profiles of phase velocity as a function of k_y at three different values of x (i.e., 14.74, 29.48, and 40.54) averaged over $t = [4500, 5000]$ shown at the top plot. The three plots that follow show the detailed time evolution (on the left y axes) of phase velocity as a function of x for three different values of k_y (i.e., 1, 3, and 5), together with the mean velocity profile shown for reference (on the right y axes). The phase velocity is computed using $v_\phi = -\partial_t \phi_{k_y}^+(x,t)/k_y$. The k_y's for which the time evolution are given and the x's for which the phase velocities are shown are marked with horizontal lines in the corresponding figures.

roughly consistent with what we see in time evolution, where coherent structures like rotating vortices are advected by zonal flows. In order for such a detailed structure to keep its coherence, the different Fourier components that make up such a structure must move at the same speed even under the action of the zonal shear.

IV. CONCLUSION

A detailed analysis of triadic interactions formulated in terms natural frequencies reveals the complex nature of the dynamics of the phases and amplitudes in the Hasegawa–Wakatani system. In particular, it is observed that a single resonant (or near resonant) triad, including a pump mode and two other modes, can saturate by adjusting the sums of phases of its legs ($\psi_{kpq}^{s_k s_p s_q} = \phi_k^{s_k} + \phi_p^{s_p} + \phi_q^{s_q}$) to be asymptotically constant, resulting in a set of nonlinearly shifted frequencies and constant amplitudes. When the interactions with zonal flows are considered, a similar saturation is possible for a single triad even without the condition of resonance. However, this solution breaks down when we add the triad, which is the reflection of the original one with respect to the y axis (or the wave-vector $\mathbf{k}$). Instead we observe three different behaviors for these triad pairs as a function of the radial wave number.

(i)   For smaller radial wave numbers, we find that the subdominant mode becomes the dominant one and grows exponentially. We call those unstable triads. They are associated with unstable subdominant modes.

(ii)   For medium radial wave numbers, after an initial growth phase, the system saturates with a more or less chaotic evolution, where the energy goes back and forth between the modes. We call these saturated triads. They are associated with weakly unstable or weakly damped subdominant modes.

(iii) For large radial wave numbers, the system decays to a steady state solution after a number of limit cycle oscillations. In some cases, these limit cycle oscillations can continue until the end of the simulation time. We call these decaying triads (even though they do not decay to zero but to a constant). They are associated with strongly damped subdominant modes.

In order to study the dynamics when those triads are connected to one another, we considered a network formulation where the wave numbers (or wave number eigenmode combinations) are considered

as nodes, and each triad represents a three body interaction. It is shown that while the zonal flow is almost never dominant in a single triad when the whole triad network with a large number of triads is considered, the zonal modes become dominant almost in each triad. Thus, the system can reach a steady state where the zonal flow dominates as the other modes decay. One interesting future perspective that is closely related is the study and the detailed understanding of the conditions for the dominance of the zonal flow as a function of the number of triads, the initial energies, their ratios, and the total energy of the network.

In terms of triadic interactions, as the zonal flow becomes dominant, it plays the role of a collective mean field; in the sense that for each mode, individual interactions with non-zonal modes start to become less important compared to the interaction with the zonal flow. This happens only when the number of triads is large enough so that the collective wins over the individual. However, this seems to happen gradually as we add triads since the contribution to the zonal flow increases with each added triad. It is interesting to note that this picture where the interaction with the zonal flow dominates over the interactions among drift waves is qualitatively consistent with that of inhomogeneous wave-kinetic formulation, where the zonal flow is treated as a collective mean field, and the direct interaction between the modes is either dropped or modeled with a diffusion operator. This actually suggests that the wave-kinetic formulation may hold beyond its strict range of validity.

Playing with the range of radial wave-numbers of the network model, we observe that when the range includes only unstable triads [i.e., (i) above] or unstable and saturated triads [i.e., (i) and (ii) above], the network system remains unstable. It saturates only when we include a sufficient range of decaying triads, with subdominant modes with $\gamma_p^+ < 0$. This means that "local coupling to damped modes" (i.e., γ_p^- modes even though $\gamma_p^+ > 0$) is not a real mechanism for turbulent saturation. However, since the fact that $\gamma_p^+ < 0$ for those modes do not come directly from dissipation but rather the detailed form of the linear growth/damping whose form is determined by various parameters including dissipation, it is correct to argue that in contrast to the Kolmogorov picture where there is an injection scale, a dissipation scale, and the inertial range in between, plasma turbulence can generate and dissipate energy in much closer scales, even though one may observe clear power law scalings.

One of the goals of the current paper was to study the effect of nonlinear synchronization of drift waves[45] on the turbulent cascade using a framework similar to the Kuramoto model,[46] which has already been attempted using simple models in fusion plasmas.[47,48] We hoped by considering a network of connected triads interacting with zonal flows, we could set up a system that would tend toward synchronization through slight nonlinear modifications of the frequencies through their interactions with the zonal flow, playing the role of the control parameter. However due to particular form of the systematic dependency of the frequencies to the wave-numbers through the dispersion relation, such a system does not seem to tend toward synchronization. It should be checked whether or not the discretization resulting from boundary conditions, for example, in cylindrical geometry, changes this picture drastically by impeding resonant interactions[49,50] especially among large scale modes.

AUTHOR DECLARATIONS
Conflict of Interest

The authors have no conflicts to disclose.

DATA AVAILABILITY

The data that support the findings of this study are available from the corresponding author upon reasonable request.

REFERENCES

[1] A. Hasegawa and M. Wakatani, Phys. Rev. Lett **50**, 682 (1983).
[2] M. Lesieur and J. Herring, J. Fluid Mech. **161**, 77 (1985).
[3] F. H. Busse and K. E. Heikes, Science **208**, 173 (1980).
[4] L. K. Currie and S. M. Tobias, Phys. Fluids **28**, 017101 (2016).
[5] A. Hasegawa and K. Mima, Phys. Fluids **21**, 87 (1978).
[6] C. Connaughton, S. Nazarenko, and B. Quinn, Phys. Rep. **604**, 1–71 (2015).
[7] P. H. Diamond, S.-I. Itoh, K. Itoh, and T. S. Hahm, Plasma Phys. Controlled Fusion **47**, R35 (2005).
[8] C. Holland, G. R. Tynan, J. H. Y. A. James, D. Nishijima, M. Shimada, and N. Taheri, Plasma Phys. Controlled Fusion **49**, A109 (2007).
[9] A. V. Pushkarev, W. J. T. Bos, and S. V. Nazarenko, Phys. Plasmas **20**, 042304 (2013).
[10] Y. Zhang and S. I. Krasheninnikov, Phys. Plasmas **27**, 122303 (2020).
[11] B. D. Scott, J. Comput. Phys. **78**, 114 (1988).
[12] A. E. Koniges, J. A. Crotinger, and P. H. Diamond, Phys. Fluids B **4**, 2785 (1992).
[13] B. Friedman and T. A. Carter, Phys. Plasmas **22**, 012307 (2015).
[14] D. D. Sarto and A. Ghizzo, Fluids **2**, 65 (2017).
[15] W. Bos, B. Kadoch, S. Neffaa, and K. Schneider, Physica D **239**, 1269 (2010).
[16] J. Anderson and B. Hnat, Phys. Plasmas **24**, 062301 (2017).
[17] F. Y. Gang, P. H. Diamond, J. A. Crotinger, and A. E. Koniges, Phys. Fluids B **3**, 955 (1991).
[18] G. Hu, J. A. Krommes, and J. C. Bowman, Phys. Plasmas **4**, 2116 (1997).
[19] R. Singh and P. H. Diamond, Plasma Phys. Controlled Fusion **63**, 035015 (2021).
[20] I. R. Goumiri, C. W. Rowley, Z. Ma, D. A. Gates, J. A. Krommes, and J. B. Parker, Phys. Plasmas **20**, 042501 (2013).
[21] J. Anderson, E-j. Kim, B. Hnat, and T. Rafiq, Phys. Plasmas **27**, 022307 (2020).
[22] R. A. Heinonen and P. H. Diamond, Phys. Rev. E **101**, 061201 (2020).
[23] N. Kasuya, M. Yagi, M. Azumi, K. Itoh, and S.-I. Itoh, J. Phys. Soc. Jpn. **76**, 044501 (2007).
[24] P. Vaezi, C. Holland, S. C. Thakur, and G. R. Tynan, Phys. Plasmas **24**, 092310 (2017).
[25] P. Donnel, P. Morel, C. Honoré, Ö. Gürcan, V. Pisarev, C. Metzger, and P. Hennequin, Phys. Plasmas **25**, 062127 (2018).
[26] A. I. Smolyakov and P. H. Diamond, Phys. Plasmas **6**, 4410 (1999).
[27] L. Chen, Z. Lin, and R. White, Phys. Plasmas **7**, 3129 (2000).
[28] S. Champeaux and P. Diamond, Phys. Lett. A **288**, 214 (2001).
[29] P. Manz, M. Ramisch, and U. Stroth, Phys. Rev. Lett. **103**, 165004 (2009).
[30] U. Stroth, P. Manz, and M. Ramisch, Plasma Phys. Controlled Fusion **53**, 024006 (2011).
[31] H. Biglari, P. H. Diamond, and P. W. Terry, Phys. Fluids B **2**, 1–4 (1990).
[32] P. W. Terry, Rev. Mod. Phys. **72**, 109 (2000).
[33] M. A. Malkov, P. H. Diamond, and M. N. Rosenbluth, Phys. Plasmas **8**, 5073 (2001).
[34] E.-J. Kim and P. H. Diamond, Phys. Rev. Lett. **90**, 185006 (2003).
[35] Z. B. Guo and P. H. Diamond, Phys. Rev. Lett. **117**, 125002 (2016).
[36] J. Kim and P. W. Terry, Phys. Plasmas **18**, 092308 (2011).
[37] J. Dominski and A. Diallo, Phys. Plasmas **28**, 092306 (2021).
[38] P. Li and P. W. Terry, Phys. Plasmas **29**, 042301 (2022).
[39] S. Xu, Z. B. Guo, and O. D. Gürcan, Phys. Rev. E **103**, 023208 (2021).
[40] H. Xia, M. Shats, and H. Punzmann, Europhys. Lett. **91**, 14002 (2010).
[41] T. Stoltzfus-Dueck, B. D. Scott, and J. A. Krommes, Phys. Plasmas **20**, 082314 (2013).
[42] M. D. Bustamante and E. Kartashova, Europhys. Lett. **85**, 34002 (2009).
[43] N. Bian, S. Benkadda, O. E. Garcia, J.-V. Paulsen, and X. Garbet, Phys. Plasmas **10**, 1382 (2003).
[44] Y. Sarazin, G. Dif-Pradalier, X. Garbet, P. Ghendrih, A. Berger, C. Gillot, V. Grandgirard, K. Obrejan, R. Varennes, L. Vermare, and T. Cartier-Michaud, Plasma Phys. Controlled Fusion **63**, 064007 (2021).

[45]D. Block, A. Piel, C. Schröder, and T. Klinger, Phys. Rev. E **63**, 056401 (2001).

[46]Y. Kuramoto, *Chemical Oscillations, Waves, and Turbulence* (Springer–Verlag, New York, 1984).

[47]S. Moradi, J. Anderson, and Ö. D. Gürcan, Phys. Rev. E **92**, 062930 (2015).

[48]S. Moradi, B. Teaca, and J. Anderson, AIP Adv. **7**, 115213 (2017).

[49]E. A. Kartashova, Phys. Rev. Lett. **72**, 2013 (1994).

[50]E. Kartashova, *Nonlinear Resonance Analysis*, by E. Kartashova (Cambridge University Press, Cambridge, UK, 2010), Vol. 1.